Advances in Science and Technology Research Journal

Advances in Science and Technology Research Journal, 2026, 20(8), 221–235
https://doi.org/10.12913/22998624/221319
ISSN 2299-8624, License CC-BY 4.0

Received: 2026.04.04
Accepted: 2026.06.01
Published: 2026.07.01

Numerical investigation of thermal performance in a solar air heater using triangular fins

Ahmed Qahtan Bahlol[1], Ansam Adil Mohammed[1*]

[1] Department of Mechanical Engineering, College of Engineering, Al-Nahrain University, Jadriya, Baghdad, Iraq
* Corresponding author e-mail: ansam.a.mohammed@nahrainuniv.edu.iq

ABSTRACT

This paper presents a study on improving the heat transfer of a flat solar collector system for air heating using a triangular fin attached on the bottom face of an absorber plate in a solar collector using a numerical simulation. A three-dimensional numerical emulation was attained utilizing a Computer simulation of fluid flow via the CFD process established on a k-ε disruption representative for renormalized array to predict the heat transfer improvement of a flat solar collector system for air heating. The numerical results acquired into a constant thermal flux 1000 W/m² and the range of Reynolds number from 2349 to 9311 were validated by comparing them with a practical data obtainable in the scientific published works. The numerical outcomes revealed that the use of triangular fins can effectively influence the thermal boundary layer by inducing periodic flow recirculation behind the fins. The numerical results also showed that at a Reynolds number of 5000 and a maximum Nusselt number of 26.0 can be reached using 10 mm fins, but applying 15 mm fins resulted in a significant increase in friction. Consequently, the thermo-hydraulic coefficient of performance (THPF) for 10 mm fins was found to be greater than 0.88 for all Reynolds numbers, making it a better choice for a solar air heating system.

Keywords: flat solar collector, triangular fins, air heater, thermal performance, turbulent.

INTRODUCTION

Solar energy constitutes one of the most considerable and prospective renewable resources obtainable to encounter the growing of global dependence for clean thermal and electrical energy [1–2]. Specifically, Baghdad is one of the regions wealthy in solar radiation that can be applied to revive the renewable energy in the region [3–4]. Therefore, among the multiplicity of technologies that harness solar radiation, solar air heaters (SAHs) enjoy notable considerable interest due to their structural simplicity, cost potency, direct applicability in space heating, drying processes and industrial ventilation [5]. In principle, the basis of a solar air heater required converting status solar radiance till thermic energy which is then transmitted to the air inflow in a channel over an absorber plate [6]. However, despited their conceptual simplicity, a traditional solar collector suffers from the intrinsically minimum thermal performance, primarily attributed to inferior coefficient of heat transfer between the absorber surface and air stream [7]. Consequently, this limitation has inspired extensive research efforts aimed at enhancing heat transfer while maintaining a reasonable pressure drop penalty. For instance, [8] suggested a heat dissipater equipped with triangular fin in an alternating design. This equalization reduced the viscous friction, allowed greater airflow, and enhanced the thermal transfer coefficient by 16.0%, compared to parallel layouts. Similarly, [9] numerically contrasted between a triangular fin, a rectangular fin and a parabolic fin shape in a tube of concentric heat exchanger, Triangular fins were established to reduce pressure drop, compared to rectangular fins. In contrast, [10] examined the influence of a triangular fin, a square fin and a circular pin fin on the flow and thermal transfer, the triangular pin fins generated extensive wakes and effective shear layers, which trapped the hot fluid and reduced local heat transfer

efficiency compared to circular fins. Furthermore, [11] studied a circular channel with depraved triangular ribs. The ribs increased air temperature by up to 17% and improved the Nusselt number by about 200% compared to a smooth pipe. Likewise, [12] investigated wavy ribs with various cross-sections, including isosceles triangular ribs, the triangular fin with isosceles appeared the greater overall thermal achievement among the shapes studied. In this context, [13] focused on the empirical relationships derived from limited experiments, while numerical simulation, particularly using Computer simulation of fluid flow via CFD, provides an effective system for examining fluid flow and heat transfer characteristics with high accuracy and considerable flexibility in varying parameters in triangular fins. Moreover, [14] experimentally investigated a dual pass solar collector with a triangular fin that attached to the bottom face of the absorber. The fins optimized the thermal transfer region, created disturbance, and reduced dead zones. In a related study, [15] designed and tested four solar air heaters: one flat plate and three with double triangular fins in different layouts (inline, staggered, and inclined staggered). They found that finned collectors outperformed the flat one, with the inclined staggered design achieving the best results, improving thermal effectiveness by a 20.7% and exergy efficiency by a 52.7%, and reducing CO_2 emissions by 14.3 tons. Additionally, [16] studied the heat transfer in triangular air passages below a heated absorber plate, using sloping fins on the sidelong walls to promote early turbulent flow. They estimated the effectiveness at equal pumping power using a parameter (hA/hsAs) and found that the fins from steel attained values of 1.71–2.04 and aluminum fins reached 2.36–2.54, depending on the dimensions of the fins, the suggested design improved the heat transfer without further pumping capacity, presentation a functional way to enhance existing solar air heaters. On the other hand, [17] investigated the natural convection in a solar air convector heater using triangular, elliptical and rectangular fins, inclined at angles of 45–90° accounting for the shadow effect by the fins, The results reveled that neglecting the shadow effect overvalued performance with a triangular and rectangular fins achieving about 10% to 20% lower performance when shadows were considered, The study also showed that the best mass flow rate occurred at fin depths of about 0.005 and 0.010 meter, the optimal depth for thermal achievements was approximately 0.025 m, beyond which improvements became negligible. Furthermore, [18] improved and tested a channel with triangular shape for a solar air convector heater with a U spin airflow type containing a novel equivalent radiation and convection loop to build an accurate mathematical model. The model miniature prediction errors for thermal efficiency and outlet temperature were reduced by 50% comparing to conventional energy balance models, strong thermal efficiency was attained at flow rate of air mass 0.045 kg/s while the best thermo-hydraulic performance come about at an internal peak angle of 60°. Also, [19] achieved an overelaborate solar air convector heater with a triangular spoiler and developed a 3D numerical pattern to estimate its achievement. The spoiler reduced the eddy regions and the temperature of the defunct zones in the flow duct to enhanced thermal performance. Collection efficiency peaked at a spoiler angle of 64°, achieving an increase of 4.4–6.2% comparing to the design without a spoiler, while a comprehensive analysis identified 40° as the optimal angle for effective efficiency. Meanwhile, [20] developed an analytical model to examine a triangular duct to a solar collector with a curving fin integrated on the absorbed plate. The fin pitch ratio was (0.05 to 0.2) and amplitude ratio was (0.025–0.125). Increasing the fin pitch ratio caused a reduction in thermal and thermo-hydraulic efficiency. However, a higher amplitude ratio improved efficiencies up to a critical Reynolds number. Additionally, [21] used ANSYS Fluent to compare a triangular fin with ribs in a solar collector and found that triangular fins alone accomplished a higher thermal performance factor due to pressure drop despite having a slightly lower Nusselt number, Parametric analysis indicated that increasing of the pitch-to-height ratio reduced the Nusselt number (Nu), friction factor (f) and thermal performance factor (THPF) while increasing the Reynolds number improved the Nusselt number and thermal performance factor. In [22], employed ANSYS Fluent to inspect triangular corrugations (continuous corrugation) on a solar air collector with pitches ranging from 55 mm to 175 mm compared with a smooth absorber plate. The corrugated surfaces showed enhancement in heat transfer, achieving a higher-level Nusselt number which increased to 199.95% at a pitch of 55 mm and Re = 3000. In [23], the shape of prismatic triangular channel solar air convector heater was examined together with a linear fins and a

quadruple rib tabulators and the governing equations were solved using a matrix inversion method in MATLAB with an average model discrepancy of 4.2%. In [24], the initial systematic examination for a shape of a triangular fin in photovoltaic thermal collectors was carried out using a 3D CFD model. Compared to a simple collector, the triangular fin design obtained 17.37% elevated thermal competence at a Reynold number (9000) and a 11.3% better than thermal capacity output at Reynold number (3000), while maintaining a similar electrical performance (13.66%). In [25], a solar collector for heating air was compared with a slanted fin in triangular and equilateral shapes. In the flow passing to a conventional rectangular duct heater under equal pumping power and geometric relation (w = 2.65 H) for equivalent conditions, the fin with triangular design achieved 7.3–25.8% higher thermal performance due to expanded effective heat transfer area. In [26], a solar air heater with forced convection and a rectangular fin as well as paraffin wax as material of a phase change (PCM) was investigated. The fins served a dual purpose of enhancing heat transfer and encapsulating PCM. In [27], theoretical and experimental analyses of a solar collector heater with a triangular fin type on the absorbed plate for enhancing the thermal transfer and reducing pressure drop with mass flow rate 0.010 kg/s were conducted. The system achieved a maximum inlet temperature of about 59 °C under a solar flux of 846 w/m². In [28], a CFD study of convex-shaped protrusions arranged in a periodic rectangular pattern on the absorber tray of a solar heater was conducted to break the viscous sublayer and enhance turbulent heat transfer. In [29], the influence of various coarseness element shapes (circular, triangular, rectangular, semicircular, square) on the performance of thermal hydraulic of a triangular passage solar heater was analyzed. At a Reynolds number of 18700 the fore chamfered of a rectangular rib (e/w = 2) produced the highest thermal and hydraulic performance parameter (THPF) of about 2.750. In [30]. V-down perforated baffles were investigated as artificial roughness in an equilateral triangular passage solar air heater varying the baffle height (5–11 mm) and open area ratio (20–29%). The highest heat transfer took place at a baffle height of about (9 mm) and open area ratio of approximately 20%, yielding a thermo-hydraulic performance factor of 2.54. In [31], an innovative solar collector for heating air with synthetic roughness in the form of alternating dimple intrusions and protrusion on the absorbed plate within a triangular passage was presented., A CFD analysis was conducted for Reynolds numbers from 4000 to 17,700, evaluating roughness parameters to optimize the performance. In [32], a flapped triangular wing swirl generators in a solar collector duct were studied, comparing backward and forward configurations with varying pitch ratios and flap angles. The forward configuration achieved a Nusselt number enhancement of 4.72–8.05 times compared to a smooth plate, with friction factor increases of 13–68.1 times. In [33], the influence of baffle positioning on the THPF of a solar heater across Reynolds number from 2370 to 8340 was explored. The conclusion demonstrated that the optimal performance depends not only on the baffle shape and geometry but critically on its placement, with the best thermo-hydraulic performance factor achieved when baffles occupy only the first 50% of the air channel.

NOVELTY IN THE CURRENT STUDY

The primary objective of the research was to investigate and enhance a numerically thermal achievement of the SAH with triangular fins arrangement. In a conventional SAH, it is known that lower heat transfer coefficients are encountered due to the occurrence of an intensive thermal boundary layer. In this research, an innovative concept of strategically modifying the geometry of SAH in such a manner that it can motivate the turbulence and reattachment of flows was proposed. The uniqueness of this research lies in its granular approach to the ratio of performance to cost. In other words, unlike other existing research which is are mostly concentrated on maximizing heat transfer, this research uniquely identifies a critical entrance for fin height (10 mm), The research also extended to the detailed characterization of the CFD analysis executed by utilizing the RNG k-ε model of turbulence and offering new insights for how triangular geometries specifically manage to achieve a more optimal balance of convective mixing and pressure drop, compared to more traditional rectangular or staggered arrangements. By validating this numerical analysis against extremely accurate experimental benchmarks, this study presented a verified a greatly efficient design solution that will bridge the gap between the theory and practice for solar heating systems.

MATERIALS AND METHODS

Geometry

The flat solar collector was designed to capture solar radiation efficiently and transform it into thermal energy through its internal components. The diagram in Figure 1 illustrates the main components and the importance of orienting it towards the south to optimize the angle of incidence of the rays. The length of the air channel is 1500 mm and the width is 750 mm. The height of air channel (the space in the between absorber plate and the bottom insulated plate) is 25 mm, with a 30 mm air distance on top of the absorber plate and a 5 mm thick glass cap. The plate of absorber is made of 0.5 mm thick aluminum and the bottom and side walls are well insulated. This design uses triangular baffles placed in the bottom face of the absorber plate at equal intervals 40 mm. The configurations follow in Figure 2(A–B) an absorber plate without fins, and an absorber plate with triangular fins attached along the entire length of duct (100%). The triangular baffles are isosceles which with the length of one side and the base of 40 mm and height of 10 or 15 mm, resulting in a vertex angle of approximately 53° for a 10 mm height and 37° for a 15 mm height. The total number of baffles is 204, distributed along the absorber plate. Regarding the CFD settings, convergence criteria were (10^{-4}) for residues and (10^{-6}) for energy and the (SIMPLE coupling algorithm), second order upwind partition schemes, 1500 iterations, mass flow inlet condition with the flow rates listed in Table 1 and a pressure outlet condition of zero (atmospheric pressure).

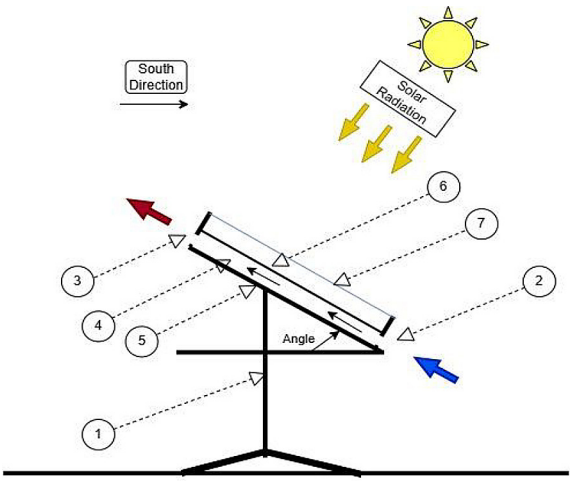

Figure 1. Schematic diagram of flat plat solar collector. metal support (1), inlet portal (2), outlet portal (3), air channel (4), insulating material (polystyrene) (5), absorber plate (6), glass cover (7)

CFD modeling

To obtain a detailed realization of the flow field and heat transfer mechanisms inside the solar collector heater, a (CFD) approach was adopted. CFD provides an efficient cost and functional alternative to extensive experimental testing that allowing for the visualization of local flow patterns, temperature distributions and pressure variations that are complicated to capture experimentally. The numerical simulations were completed using a finite volume method where the dominant equations of momentum, continuity and energy were solved iteratively unto convergence. A structured of hexahedral mesh was generated with refined elements near the walls to properly resolve the boundary layer and establishing the wall distance (y+) remained close to unity, all simulations were carried out under steady state conditions assuming incompressible flow and constant thermo-physical properties estimated at the mean bulk temperature. Table 1 specifies the boundaries and physical properties for both working fluid and material. This numerical framework authorizes a systematic comparison of the different baffle configurations under identical operating conditions and providing dependable data for the subsequent analysis of the thermal and hydraulic performance.

The simultaneous application of a constant temperature condition on the top plate and insulating walls on the sides and bottom accurately simulate a real solar collector, where:

- Solar radiation heated only the absorber plate.
- Insulation prevents heat loss from other directions.
- All incoming heat is transferred by convection to the passing air.

Mesh independence

In line with the mesh independence test outcome summarized in Table 2 and Figure 3, a systematic grid refinement research was assumed to achieve the best mesh resolution with equilibrium computational accuracy and resource efficiency. The cell count was progressively increased from approximately 1.22 million to an over 7.83 million, and the corresponding variations in the outlet temperature and convective heat transfer

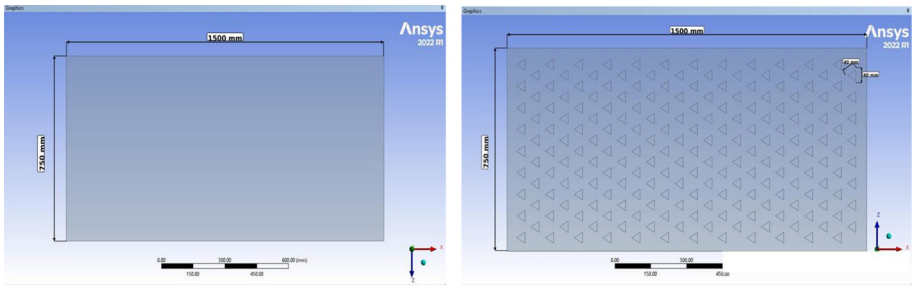

Case A **Case B**

Figure 2. Cases of the studied of solar collector air heater with dimensions: (A) Smooth plate (without Baffles); (B) finned absorber plate

Table 1. Boundary condition and material properties

Reynold NO.	2364–9311	Aluminum density (kg/	2719
ṁ (kg/s)	0.017–0.06	Aluminum thermal conductivity (K) (W/m·k)	202.4
Side heat flux (Q) (W/m^2)	(0) adiabatic	Aluminum Specific heat(cp) (J/kg·K)	871
Heat flux at absorber plate (Q) (W/m^2·K)	1000	(Insulation) polystyrene density (kg/m^3)	20
Turbulence model in ANSYS	RNG-k-ε model with enhancement wall treatment	polystyrene thermal conductivity (K) (W/m·K)	0.03
		Polystyrene Specific heat(cp) (J/kg·K)	1400
Air density (kg/m^3)	1.167	Air thermal conductivity (K) (W/m·K)	0.0262
Air viscosity (kg/m·s)	1.85 × 10^{-5}	Air specific heat (cp) (J/kg·K)	1006

coefficient were closely observed. The results indicate that beyond a threshold of approximately 2.07 million cells, further refinement yields minor changes in the predicted parameters with deviations in the outlet temperature and heat transfer coefficient falling below 2% and 3%, respectively. Consequently, the mesh configuration comprising approximately 2.07 million cells was chosen for all following simulations, as it achieved a favorable settlement between the solution fidelity and the computational economy. This selection verified that the numerical predictions awerere sufficiently independent of the mesh resolution, thus enhancing the reliability of the simulated thermo-fluid characteristics.

Code validation

To validate the existing CFD a numerical simulation was accomplishing and compared with an experimental measurements obtained from a specially designed test apparatus [33]. The verification was completed with a rectangular barriers positioned in the second and last part of the absorbed plate under identical operating conditions as shown in Figure 4 and two mass flow rates were applied (0.017 kg/s - 0.025 kg/s) with corresponding solar irradiance values of 670 W/m² and 982 W/m², respectively. The temperature of air distribution along the flow direction (x-direction) surmised by the CFD model was extracted and compared

Table 2. Mesh independence trial

Cell No.	Tout(K)	h (W/m^2·K)	Deviation percentage of tout (%)	Deviation percentage of h (%)
1,222,402	318.460	22.93	-	-
1,562,164	318.358	22.960	0.0320	0.1308
2,068,934	**318.265**	**22.966**	**0.0292**	**0.0261**
3,304,647	318.194	23	0.0223	0.1480
7,829,605	318.022	22.734	0.0541	1.1565

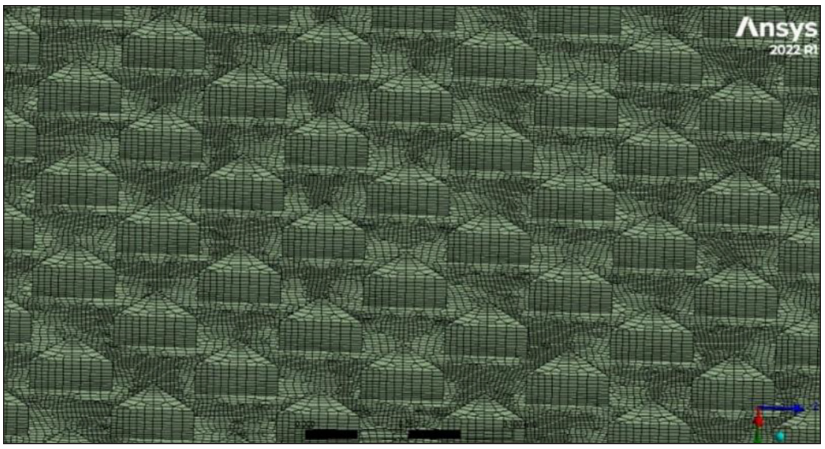

Figure 3. Arrangement of computational network for the simulated modeling

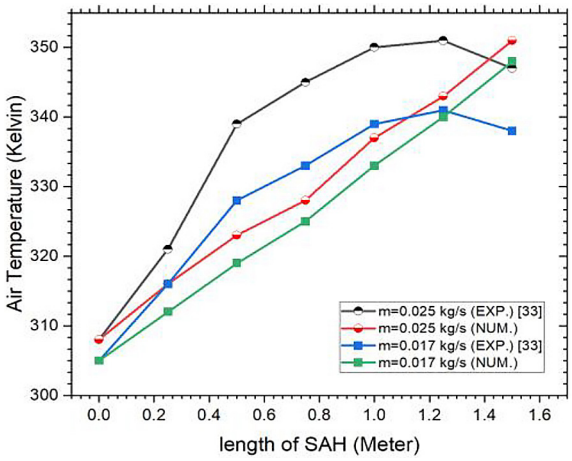

Figure 4. Comparison of the CFD outcome and the experimental data

with thermocouple readings at the same longitudinal positions, the results of temperature curves predominantly identify the experimental directions with absolute deviations ranging from 5.2% to 0.65%. This level of the agreement confirms that the proposed computational fluid dynamics methodology including the RNG k-ε disruption model and the adopted partitioning strategy was capable of accurately simulating the thermal attitude of the triangular barrier in solar heater. Therefore, the clarified numerical model was considered reliable for further parametric analyses of the remaining triangular barrier configurations.

Governing equations and data reduction

A numerical consideration to a thermal rendering of a solar heater with a triangular fin was conducted under a condition of steady state, three dimensional and incompressible turbulent flow conditions. The thermo-physical characteristic of the air was presumed constant at the mean bulk temperature and the radiative heat transfer was neglected within the computational domain. The Reynolds-averaged Naiver-Stokes (RANS) approach was employed with a turbulence model of RNG k-ε was selected based on validation against standard correlations.

- Continuity equation – the equation of mass conservation for the fluid (air) is expressed as [34]:

$$\frac{\partial \rho u_i}{\partial x_i} = 0 \ (1) \tag{1}$$

where: u_i symbolizes the components of velocity in x_i direction.

- Momentum equations – the equation of momentum conservation for the turbulent flow field is given by:

$$\frac{\partial}{\partial x_j}\left(\rho u_i u_j\right) = -\frac{\partial p}{\partial x_i} + \\ + \frac{\partial}{\partial x_j}\left[\mu\left(\frac{\partial u_i}{\partial x_j} + \frac{\partial u_j}{\partial x_i}\right) - \frac{\rho u'_i}{u'_j}\right] \tag{2}$$

where: ρ – air density, p – static pressure, μ – dynamic viscosity and $(-\frac{\rho u'_i}{u'_j})$ is the Reynolds stress tensor, which is modeled using the turbulence model.

- Energy equation – the equation of energy conservation for the fluid and solid domains is expressed as:

$$\frac{\partial}{\partial x_i}\left(\rho u_i C_p T\right) = \frac{\partial}{\partial x_i}\left(\lambda \frac{\partial T}{\partial x_i}\right) \tag{3}$$

For the solid region (absorber plate, triangular fins and bottom plate), the heat conduction equation is:

$$\frac{\partial}{\partial x_i}\left(\frac{\lambda s \partial T}{\partial x_i}\right) = 0 \quad (4)$$

where: C_p specific heat at constant pressure, λ and λ_s are the thermal conductivities of the fluid and solid, respectively, and T is the temperature.

- Turbulence model (RNG k-ε) – on the basis of the validation presented in the reference paper, the RNG k-ε model was adopted to account for turbulent flow effects. The equations for turbulent kinetic energy k and its dissipation rate ε are [35]:

$$\frac{\partial}{\partial x_i}(\rho k u_i) = \frac{\partial}{\partial x_j}\left(\frac{\alpha k \mu_{eff} \partial k}{\partial x_j}\right) + Gk - \rho\varepsilon \quad (5)$$

$$\frac{\partial}{\partial x_i}(\rho \varepsilon u_i) = \frac{\partial}{\partial x_j}\left(\frac{\alpha \varepsilon \mu eff \partial \varepsilon}{\partial x_j}\right) + \frac{C1\varepsilon\varepsilon}{k G_k} - \frac{C2\varepsilon\rho\varepsilon^2}{k} \quad (6)$$

where: G_k is the generation of turbulence kinetic energy due to mean velocity gradients, $\mu_{eff} = \mu + \mu_t$ is the effective viscosity, and the model constants were derived from the RNG theory.

- Performance evaluation parameters – the thermal-hydraulic performance of the triangular finned solar heater was evaluated using the following parameters [36,37]:
- Reynolds number

$$Re = \frac{\rho U D_h}{\mu} \quad (7)$$

where: U is the average air velocity and D_h is the hydraulic diameter of the triangular flow passage.

- Nusselt number – the local and average Nusselt numbers are computed as:

$$Nu_x = \frac{h_x D_h}{k} \quad (8)$$

$$Nu = \frac{1}{S\int Nu_x}\, dS \quad (9)$$

where: h_x is the local convective heat transfer coefficient:

$$h_x = \frac{q}{T_{w,x} - T_{b,x}} \quad (10)$$

- Friction factor

$$f = \left(\frac{\Delta P}{L}\right)\frac{\rho U^2 D_h}{2} \quad (11)$$

- Thermo-hydraulic performance factor (THPF) [38]

$$THPF = \frac{Nu/Nu_S}{(f/f_S)^{\frac{1}{3}}} \quad (12)$$

where: Nu_s and f_s correspond to the smooth absorber (without fins).

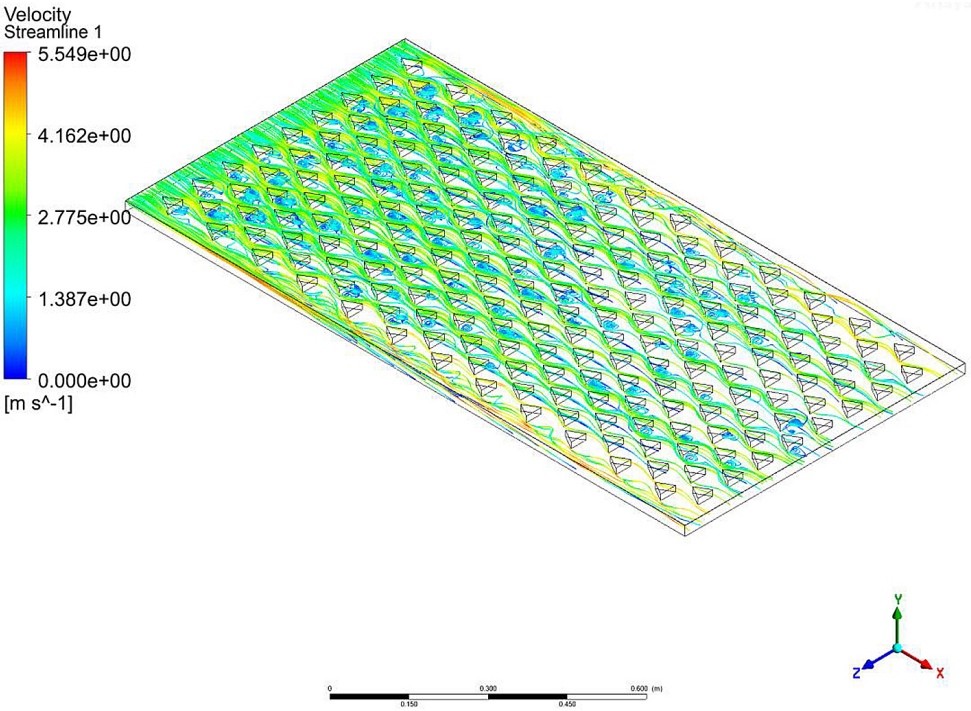

Figure 5. Velocity streamlines within the air duct with triangular fins

RESULTS AND DISCUSSION

Velocity streamline patterns

Figure 5 illustrates the three-dimensional velocity streamline distributions within the solar heater duct for the triangular-finned absorber plate exhibits a substantially altered flow structure. As the air stream encounters each triangular fin, the streamlines converge and accelerate over the fin apex due to the local reduction in flow area. Downstream, a featured recirculation zone forms instantly, distinguished by closed low velocity streamlines that indicate flow separation and wake development. These recirculating regions are restricted to the inter fin cavities and periodically iterate along the channel length. The streamline curvature shows a periodic pattern of alternating acceleration and deceleration which encourage continuous disturbance of the thermal boundary layer. Additionally, the three-dimensional path of the streamlines shows the confirmation of secondary flows in the span-wise direction that improves the fluid exchange between the nearby wall zone and the core of the flow. This behavior confirms that the triangular fins act as an effective passive turbulence performers and increasing convective mixing while maintaining a relatively organized flow structure compared to more aggressive tabulators. The situation of the streamline topology directly supports the subsequent quantitative detecting of enhanced Nusselt number and thermo-hydraulic performance in the finned arrangement.

Velocity vector field analysis

Figure 6 indicates a two-dimensional velocity vector field draw out from an absorbed plate in a solar air heater linked together with a triangular fin, the vectors are color coded according to their velocity values extend from zero (dark blue) to approximately 9.02 m/s (dark red) that provide a detailed perception of the localized flow structure resulting from the fin geometry. The vector field shows a featured pattern of flow acceleration and deceleration around each triangular fin. As the incoming air and approaches to the frontal edge of the fin, the stream lines converge and the vector magnitude increases, clearly indicating like a jet localized acceleration due to the reduced cross sectional area of the flow. Above the top fins, the vectors are densely congested and run almost parallel to the fin surface and reflecting the region of highest velocity, directly downstream of the fins, a distinct recycling region is observed where the vector directions reverse and form a closed vortex. This vortex region is characterized by low velocities (blue vectors) and a rotational motion that continues for a distance approximately equal to the distance between the fins before the flow returns to the absorber plate. These recycling regions represent a crucial role in heat management. By trapping the fluid, these zones enhance the mixing between the hot wall bound area and the coldish flow. The alternating pattern of acceleration and deceleration along the channel ensures a periodic disturbance in thermal boundary layer and prevent it from excessive growth. Furthermore, the vector field display a slight upward deflection of the flow after each fin contributing to the three dimensional nature of the flow and enhancing the fluid exchange along the channel. This behavior is particularly proof in the overlapping arrangement, where the vectors exhibit a gentle sinuous path, rather than a purely longitudinal alignment. From a hydrodynamic point of view, the vector field also explains the pressure losses associated with the fins. The expansion behind each fin generates a pressure retrieval zone, but the energy dissipated in the recirculation zones contributes to the overall coefficient of friction. However, the vector structure shows that the triangular shape produces a relatively compact turbulence zone compared to other geometries characterized by a favorable equilibrium between mixing intensity and pressure drop. The observed flow structure directly confirms the develop of convection heat transfer that measured by the Nusselt number where the periodic vortex motion efficiently transfers thermal capacity from the absorbed plate to the airflow.

Temperature distribution pattern

Figure 7 shows a temperature contour that plots on the face surface of the absorbed plate with the triangular finned shapes; the temperature field exhibits a clearly different behavior. The introduction of triangular fins disrupts the uniform thermal pattern creating distinguished localized temperature gradients around each fin. The contour lines showed cooler zones downstream of the fins corresponding to the regions where the recirculating flow entrains cooler air towards the heated surface. This intermittent

renewal of the thermal boundary layer prevents the sustained temperature build up notice in the smooth duct. Additionally, the fin surfaces display a nearly isothermal characteristic, indicating efficient heat conduction from the absorbed plate into fins thereby extending the effective heat transfer area, the temperature gradients between the fin tips and the inter fin cavities are steep, signifying high local heat fluxes. Moreover, the span-wise temperature variation is more declared in the finned case, suggesting that the fins achieve a three dimensional thermal field with enhanced mixing across the channel width, the overall temperature level on the absorber plate is lower in the finned shapes under identical operating conditions directly correlating with the improved convective heat removal. These thermal field examinations provide an understandable mechanistic explanation for the higher Nusselt numbers and enhanced thermal efficiency achieved with triangular fins, as the periodic disarrangement of the thermal boundary layer and the increased in superficies area collectively augment the energy transport to the air channel.

Influence of the fin height on convective heat transfer coefficient

Figure 8 presents the difference in the convection heat transfer coefficient (h) with the Reynolds number (Re) for a smooth absorber plate and for configurations of triangular fins at heights of 10 mm and 15 mm, the data cover the ambit of Reynolds number from 2349 to 9311 and include typical transition and turbulent flow systems for solar air heater operation. In all configurations, the heat transfer coefficient rises steadily with Reynolds number with enhancement in turbulent mixing and thinning on the thermal boundary layer at high flow velocities. The smooth channel expresses the lowest values of h, ranging approximately from 6.7 W/m²·K at Re = 2349 to 15.8 W/m²·K at Re = 8296, This standard behavior reflects the inherent limitation of a flat absorber plate, where heat transfer relates entirely on the natural development of the boundary layer without any deliberate flow turbulence, the integration of triangular fins results in a substantial increase in the heat transfer coefficient across the entire Reynolds number range. For 10 mm fin heights, the heat transfer coefficient increases from approximately 9.5 W/m²·K at 2636 to 20.5 W/m²·K at 9311, representing a 42–63% improvement compared to the smooth plate; 15 mm fins obtain even higher values of h, reaching 10.8 W/m²·K at the lowest Reynolds number and 22.5 W/m²·K at 8631, corresponding to improvements of 61–74% compared to the smooth plate. The performance improvement is most declared at lower Reynolds numbers, where the fins disrupt the formed boundary layer more effectively and

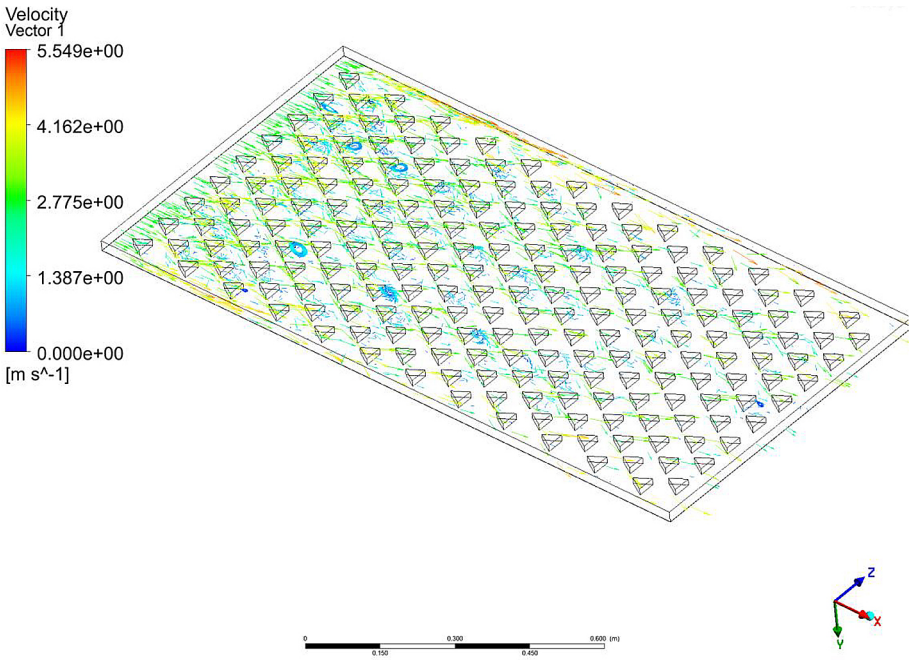

Figure 6. Velocity vector within the air duct with triangular fins

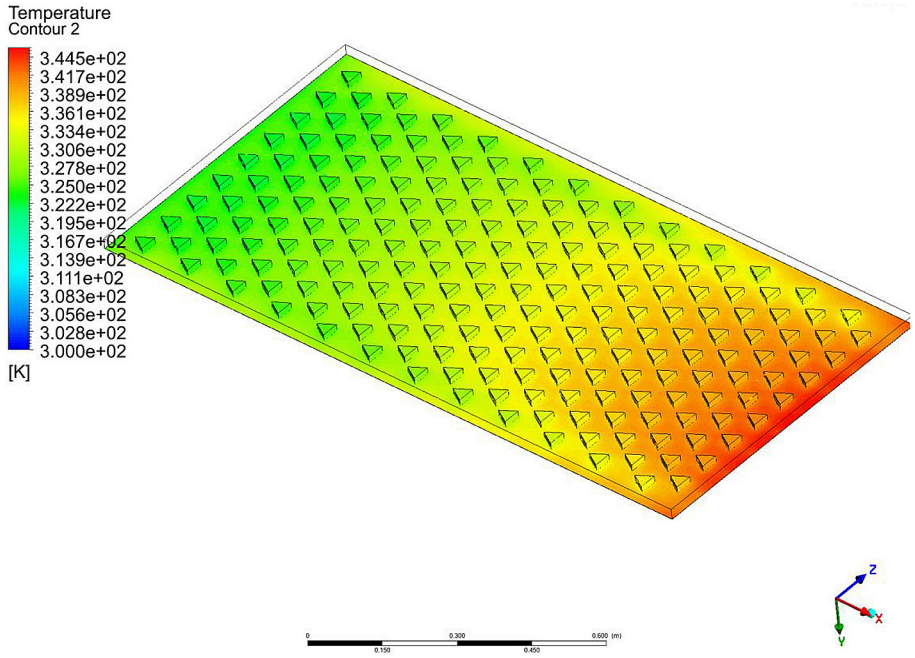

Figure 7. Temperature contour using triangular fin

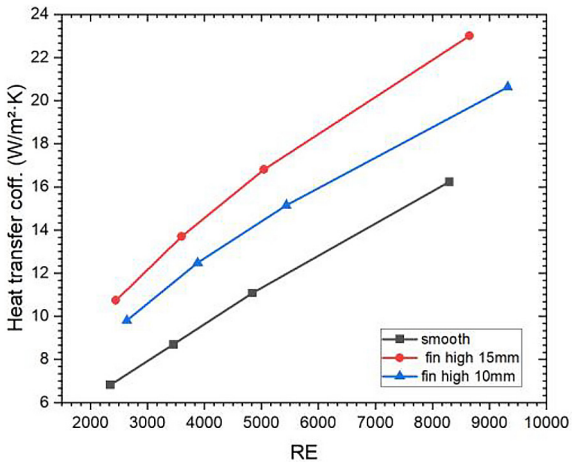

Figure 8. Variation of heat transfer coefficient with Reynolds number for a smooth and triangular fins attached in absorber plates at fin heights of 10 mm and 15 mm

this improvement remains significant under fully turbulent conditions. The observed direction demonstrates that increasing fin height enhances heat transfer by providing a major efficient surface area and generating a stronger flow separation and recirculation. The longer fins protrude more importantly into the flow core intensifying local velocity gradients at the fin tips and contribute to more pronounced vortex decoupling downstream. However, this improvement is followed by a greater pressure drop, which will be addressed in the subsequent thermal performance analysis. It is noticeable that the difference in h between the two fin heights decreases with increasing Reynolds number, indicating that at prominent flow rates, the mixing achieve of the 10 mm fins becomes sufficiently strong to reduce the benefit of increasing fin height. This observation confirms the significance of optimizing fin geometry to equilibrium heat gains and hydraulic losses. Overall, the quantitative trends in Figure 9 confirm that triangular fins are highly effective in improving the convection heat transfer in solar heaters with longer fins providing a greater optimization, especially in the transition flow systems. These results provided a basis for the subsequent thermo-hydraulic performance factor evaluation where the trade-off between increased heat transfer and pressure drop is systematically estimated.

Nusselt number characteristics

Figure 9 expresses the variation of the Nusselt number (Nu) with Reynolds number for a smooth absorber and the two triangular finned shapes (fin heights of 10 mm and 15 mm). The Nusselt number represents the convective heat transfer rate and is the key to indicator for the thermal performance. For all configurations, Nusselt number increases along with Re, as expected due to enhanced turbulent mixing and boundary layer thinning. The smooth duct expresses the lowest Nu across the entire range, rising from

approximately 12.5 at Re = 2349 to about 20.0 at Re = 5000, the addition of triangular fins significantly raises Nu, confirming the effectiveness of extended surfaces in augmenting heat transfer. However, a notable observation is that the 10 mm fins consistently reach a higher Nu values than the 15 mm fins despite their smaller height. At Re = 2636 Nusselt number for the 10 mm fin height is 17.0, compared to 16.0; for the 15 mm fins at Re = 5000 the values are 26.0 and 25.0, respectively. This apparently counterintuitive result can be described by examining the flow structure. As clarified in the velocity vector field (Figure 7) and streamline patterns (Figure 6) the triangular fins induce periodic flow separation and recirculation zones, for the heightened fins (15 mm), the recirculation regions become larger and more persistent of creating zones where hot fluid becomes trapped between fins, thereby reducing the local convective heat transfer effectiveness, The 10 mm fins generate a more compact wake that promotes efficient renewal of the thermal boundary layer without causing any excessive stagnation. Furthermore, the heightened fins may experience a lower fin efficiency due to a longer conductive path, slightly decreasing the effective heat transfer from the fin surface.

Friction factor features

Figure 10 presents the difference of the friction factor (f) with the Reynolds number for the smooth duct and the two finned configurations (fin heights of 10 mm and 15 mm). The friction factor is a measure of the pressure drop per unit length and is inverted to the hydraulic penalty introduced by the triangular fins. For all cases, f decreases when the Reynolds number increases, which is typical of turbulent and transitional flow in ducts. The smooth duct shows the lowest friction factor dropping from 0.016 at Re = 2349 to 0.008 at Re = 8296, the insertion of a triangular fins causes a primary rise in the friction factor due to flow separation wake formation and increased surface area. At Re = 2636, the 10 mm fins height yield f=0.044, approximately 2.75 times higher than the smooth plate, while the 15 mm fins give f=0.065 about 4.06 times higher value. The variance narrows slightly at higher Reynolds numbers, but the higher fins consistently impose a greater pressure drop penalty. The higher friction factor for the 15 mm fins is directly related to more intense flow recirculation and larger wake regions observed in the velocity vector field (Figure 7). The higher fins protrude deeper to the center flow, leading to stronger flow blockage and increased turbulent dissipation. Although this enhances heat transfer (as seen in Figure 9), the associated rise in pumping power requirement is disproportionately high. The data in Figure 11, in conjunction with the thermo-hydraulic performance factor (THPF) shown in Figure 12, confirm the necessity of balancing thermal gains against hydraulic losses. While the 15 mm fins provide higher-level of convective heat transfer coefficients, their high friction factor leads to a lower THPF compared to the 10 mm fins, particularly at elevated Reynolds numbers. Hence, from a practical design point of view, the 10 mm triangular fins represent a more efficient configuration for the solar air heater application.

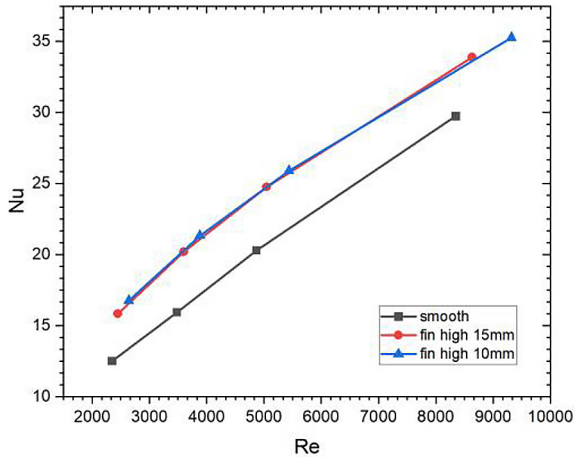

Figure 9. Nusselt number against Reynolds number for a smooth absorber and triangular finned absorber plates

Thermo-hydraulic performance factor

Figure 11 illustrates the difference of the THPF with Reynolds number for the two finned configurations (fin heights of 10 mm and 15 mm). This parameter equipping a balanced appreciation of the net earning achieved by adding fins considering for both the strengthening in convective heat transfer and the accompanying raise in the friction losses. For both fin heights, the THPF declines monotonically, decreasing as the Reynolds number raises from 2446 into 9311, the 10 mm fins high consistently display higher THPF values, ranging from approximately 0.99 at Re = 2636 to 0.88 at Re = 9311, whereas the 15 mm fins show lower values, decreasing from 0.81 to 0.64 at Re = 2446 to 8631. This direction indicates that the higher

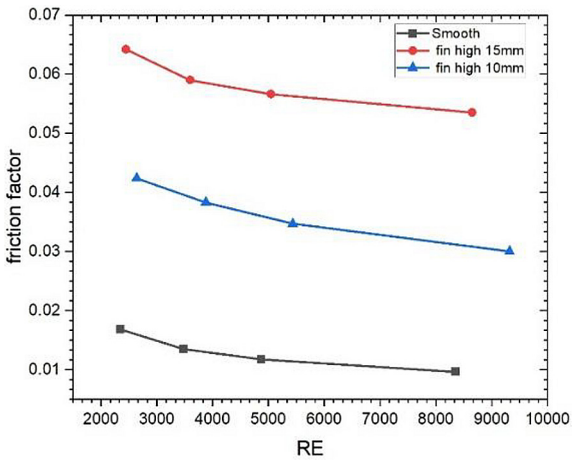

Figure 10. Friction factor against Reynolds number for smooth absorber and triangular finned absorber plates

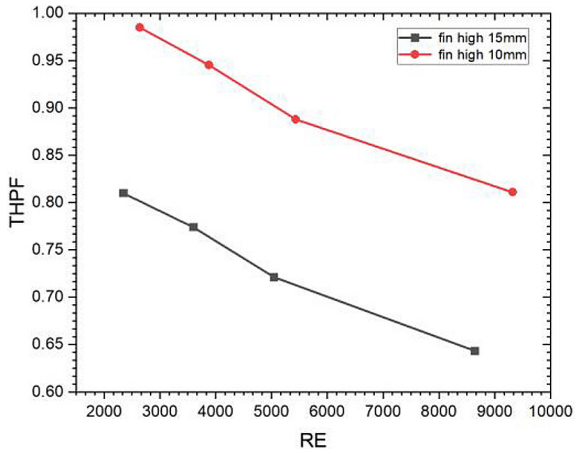

Figure 11. Thermo-hydraulic performance factor contra Reynolds number for triangular finned absorber plates

fins, despite providing a higher convective heat transfer coefficient, as seen in Figure 9, cause a disproportionately larger friction retribution which offsets much of the thermal gain. The higher THPF of the 10 mm fins is directly supported by the Nusselt number and friction factor data presented in Figures 10 and 11. Although the 15 mm fins generate stronger flow disruption and larger recirculation zones, these effects lead to excessive pressure drop without a proportional increase in heat transfer. The 10 mm fins strike a more appropriate balance, yielding significant heat transfer augmentation, while maintaining a more moderate pressure drop penalty. From a point of view of practical design, a THPF greater than 0.8–0.9 is generally considered to denote a performance improvement over the smooth plate. The 10 mm fins maintain the THPF values above 0.88 across the entire Reynolds number range, confirming their effectiveness for solar air heater applications. In contrast, the 15 mm fins height drop below 0.7 at higher Re, making them less adequate despite their higher geometry. These results confirm the importance of geometric optimization, demonstrating that increasing of fin height does not guarantee better overall performance.

STUDY LIMITATIONS

The current research concentrated exclusively on the effectiveness of fin height holding both the fin spacing (40 mm) and channel height (25 mm) constant. The sensitivity analysis of the results is based on the fin spacing (Fin Spacing = 40 mm). The fin spacing defined the length of the recirculation zone behind each fin, if the spacing is too slight, amounting to approximately 20 mm, the recirculation zones may overlap and merge, which reduces the thermal regeneration efficiency of the boundary layer. If the spacing is large, reaching about 80 mm, the flow will return to its normal streamlined behavior before reaching the following fin, reducing the accumulated benefit of the fins. The optimal fin height of 10 mm may vary slightly if the fin spacing is altered, but the general principle is that moderately high fins, rather than very high ones, achieve maximum total thermal power (THPF). The channel height limits the amount of space available for flow and the percentage of channel breakthrough by the fins. For 10 mm fins, they penetrate approximately 40% of the channel height and for 15 mm fins, they penetrate 60% of the channel height. The 10 mm fins will have a relatively lower penetration (only 37.5%); therefore, their performance may progress because they cause less flow obstruction. Conversely, if the channel height is reduced, the 10 mm fins will be closer to the top surface, which may cause considerable obstruction and an increase in the coefficient of friction. The judgment that 10 mm fins are better than 15 mm fins depends on a constant channel height 25 mm. In higher channels, 15 mm fins may become additionally efficient. In shorter channels, 5 mm fins may become optimal. Therefore, the present result should be explained in the case of the fin penetration ratio (fin height / channel height), not the absolute fin height. Only isosceles triangular fins were used and the apex angle as well as aspect ratio were not changed. On the basis of

the presented results, despite the limitations mentioned, the following guidelines can be offered to engineers and designers:

1. Recommended penetration ratio – to gain the best THPF in a solar collector with triangular fins a specific penetration ratio is recommended (fin height/channel height), ranging from 0.3 to 0.45. In this study, 10 mm fins achieved a ratio of 0.4, which was optimal.
2. Avert high ratios – penetration ratios exceeding 0.55, such as 15 mm fins in a 25 mm channel (a ratio of 0.6) lead to disproportionate hydraulic losses and THPF regression due to hot fluid retention.
3. Use the THPF coefficient as a key indicator – Nusselt optimization alone should not be depended upon, performance should always be evaluated using the THPF which balances thermal attained and pressure losses.
4. Future studies are needed – to provide more comprehensive design guidance this study recommends further parametric analyses that include variations in fin spacing, channel height and fin tip angle.

CONCLUSIONS

The current research presented a numerical investigation that provided a comprehensive appreciation of the thermal hydraulic implications of integrating a triangular fin in the solar heater (SAH) systems. On the basis of the validated 3D CFD simulations across a Reynolds number range from 2349 to 9311, the following conclusions were drawn, with particular emphasis on the fundamental tradeoff between thermal enhancement and pressure losses:

Primary scientific contribution optimal fin height trade off: The essential contribution of this study was the identification of a non-linear and non-monotonic relationship between fin height and system efficiency. While the 15 mm fins produced the elevated absolute Nusselt numbers (indicating superior convective heat transfer), they also induced a disproportionately high increasing in friction factor (up to 4.06 times that of a smooth plate at low Re). This extravagant flow blockage and pressure drop penalty severely degrades their net useful energy earning. In contrast, the 10 mm fin arrangement achieves a superior thermo-hydraulic performance factor (THPF > 0.88 across all Re) and provides the optimal balance by enhancing heat transfer without incurring prohibitive hydraulic losses.

The integration of triangular fins effectively counters the low heat transfer coefficients model of a smooth absorber plate SAHs. The geometry of the fin strength, periodic separation and reattachment of the airflow prevent the development of a thick thermal boundary layer and promote a large convective mixing near the absorber surface.

A critical discovery of this study was the nonlinear relationship between fin height and overall efficiency. While the 15 mm fins presented the highest absolute Nusselt numbers, they also introduced disproportionate pressure drops due to excessive flow blockage. However, the 10 mm fin configuration emerged as the optimal design, maintaining a THPF above 0.88. This mention that moderate surface protrusions are more effective for solar thermal applications where fan power consumption is a limiting characteristic.

The RNG k-ε turbulence model successfully captured the complex vortex structures that generated behind the triangular summit. The results manifest that enhanced in heat transfer is primarily driven by the recirculation regions which increase the residence time of the air in high flux regions without causing the extreme stagnation observed in higher fin profiles.

From an engineering viewpoint, the using of 10 mm triangular fins introduced a strong and scalable method for enhancing the energy density of solar collectors. The appropriate balance between thermal gain and friction penalty makes this arrangement highly compatible for sustainable space heating and industrial drying processes, providing a verified benchmark for future experimental prototypes.

REFERENCES

1. Mohammed A.A., Abbas A.M., Al-Gburi H. Experiment investigating the effect of ZnO nano-particles on diesel engine performance and emissions. Adv. Sci. Technol. Res. J. 2026;20(1):491–500. https://doi.org/10.12913/22998624/211614
2. Abbas M.F., Mohammed A.A., Mohammed A.A., Channapattana S., Parlak Z. Geothermal energy development in Türkiye: A review. Al-Nahrain J. Eng. Sci. 2024;27(2):207–225. https://doi.org/10.29194/NJES.27020207
3. Mohammed A.A., Ali M.A., Alkhafaji M.H. Numerical and experimental modeling of a low cost square pyramid solar still in Baghdad. Heat Transfer. 2026;

https://doi.org/10.1002/htj.70195

4. Al-Obaidi Q., Mahmoud M.S., Nabil R. Study of prototypes for biofuel production Extraction from biodegradation in oxygen-free environments Processing Wastewater. Sol. Energy Sustain. Dev. J. 2025;14(1):522–539. https://doi.org/10.51646/jsesd.v14i1.418
5. Jaber M.W.K., Ghafoor Q.J.A., Mohammed A.A., Mahmoud M.S., Khudheyer A.F. Optimizing the size for solar parabolic trough concentrator numerically. Int. J. Mech. Eng. 2022;7(1):610–615.
6. Pathak S.K., Tyagi V.V., Chopra K., Pandey A.K., Goel V., Saxena A., Ma Z. Energy, exergy, economic and environmental analyses of solar air heating systems with and without thermal energy storage for sustainable development: A systematic review. J. Energy Storage. 2023;59:106521. https://doi.org/10.1016/j.est.2022.106521
7. Mustafa A.W., Jawad I.R., Mohammed A.A. Constructal design of cross-flow heat exchanger with concave/convex fins. Heat Transfer. 2025;54(1):21–40.https://doi.org/10.1002/htj.23158
8. Chu W.-X., Lin Y.-C., Chen C.-Y., Wang C.-C. Experimental and numerical study on the performance of passive heat sink having alternating layout. Int. J. Heat Mass Transf. 2019;135:822–836. https://doi.org/10.1016/j.ijheatmasstransfer.2019.02.034
9. Kumar S., Karanth K.V., Murthy K. Numerical study of heat transfer in a finned double pipe heat exchanger. World J. Model. Simul. 2015;11(1):43–54.
10. Ambreen T., Saleem A., Park C.W. Pin-fin shape-dependent heat transfer and fluid flow characteristics of water- and nanofluid-cooled micropin-fin heat sinks: square, circular and triangular fin cross-sections. Appl. Therm. Eng. 2019;158:113781.https://doi.org/10.1016/j.applthermaleng.2019.113781
11. Hammoodi K.A., Hasan H.A., Abed M.H., Basem A., Al-Tajer A.M. Control of heat transfer in circular channels using oblique triangular ribs. Results Eng. 2022;15:100471. https://doi.org/10.1016/j.rineng.2022.100471
12. Wang L., Lv C., Liu X., Mao J., Zhang D., Liu Y., Li M. Research on improving heat transfer performance by using wavy ribs with different cross sections. Appl. Therm. Eng. 2024;257:124397. https://doi.org/10.1016/j.applthermaleng.2024.124397
13. Imran M., Lau K.K., Ahmad F., Laziz A.M. A comprehensive review of Computational Fluid Dynamics (CFD) modelling of membrane gas separation process. Results Eng. 2025;26:105531. https://doi.org/10.1016/j.rineng.2025.105531
14. Machi M.H., Al-Neama M.A., Buzás J., Farkas I. Energy-based performance analysis of a double pass solar air collector integrated to triangular shaped fins. Int. J. Energy Environ. Eng. 2022;13(1):219-229. https://doi.org/10.1007/s40095-021-00422-z
15. Albdoor A.K., Obaid Z.A.H., Kamel M.S., Azzawi I.D. Energy, exergy, economic and environmental analysis of a solar air heater integrated with double triangular fins: Experimental investigation. Int. J. Thermofluids. 2024; 24:100979. https://doi.org/10.1016/j.ijft.2024.100979
16. Karwa R. Enhanced heat transfer performance of multiple triangular air flow passages in parallel with inclined fins for flat plate solar air heater. J. Sol. Energy Eng. 2022;144(5):051003. https://doi.org/10.1115/1.4053976
17. Hosseini S.S., Ramiar A., Ranjbar A.A. The effect of fins shadow on natural convection solar air heater. Int. J. Therm. Sci. 2019;142:280–294. https://doi.org/10.1016/j.ijthermalsci.2019.04.015
18. Akhbari M., Rahimi A., Hatamipour M.S. Modeling and experimental study of a triangular channel solar air heater. Appl. Therm. Eng. 2020;170:114902. https://doi.org/10.1016/j.applthermaleng.2020.114902
19. Cai Q., Jia B., Liu F., Yu H., Liu J., Chen B., Wang H. Influence of triangular spoilers on the performance of serpentine solar air heaters. Numer. Heat Transf. A Appl. 2025;86(6):1628–1641. https://doi.org/10.1080/10407782.2023.2280196
20. Renald T.C.J., Somasundaram P., Matheswaran M.M., Gnanasekaran N. Analytical investigation on thermo hydraulic performance augmentation of triangular duct solar air heater integrated with wavy fins. Int. J. Green Energy. 2023;20(5):544–554. https://doi.org/10.1080/15435075.2022.2111215
21. 21. Singh V., Yadav V.S., Trivedi V., Singh P. Performance enhancement of the triangular fins solar air heater by adding ribs on the side wall and middle section of absorber plate. Proc. Inst. Mech. Eng. A J. Power Energy. 2026; https://doi.org/10.1177/09576509261426237
22. Prajapati S., Naik N. Numerical solution of solar air heater with triangular corrugations for indirect solar dryer: Influence of pitch and an optimized pitch of corrugation for enhanced performance. Sol. Energy. 2022;243:1–12. https://doi.org/10.1016/j.solener.2022.07.044
23. Stalin P.M.J., Rao P.N., Palaniappan M., Kumar P.M., Udhayakumar K. Effective thermal performance assessment for prismatic triangular solar air heater integrated with fins and turbulators. Numer. Heat Transf. A Appl. 2025;86(22):8129–8145. https://doi.org/10.1080/10407782.2024.2357592
24. Hamida M.B.B., Khelifa A., Attia M.E.H., Abdel-Aziz M.M. Maximizing energy output in PVT systems with triangular-finned solar air collectors. Appl. Therm. Eng. 2025;278:127247. https://doi.org/10.1016/j.applthermaleng.2025.127247
25. Karwa R. Performance of finned absorber plate solar air heater having multiple triangular air flow passages in parallel under transition to turbulent flow condition.

J. Sol. Energy Eng. 2024;146(2):021006. https://doi.org/10.1115/1.4063494

26. Balakrishnan P., Vishnu S.K., Muthukumaran J., Senthil R. Experimental thermal performance of a solar air heater with rectangular fins and phase change material. J. Energy Storage. 2024; 84:110781. https://doi.org/10.1016/j.est.2024.110781
27. Singh P., Yadav V.S., Sudhakar T., Trivedi V., Singh V. Performance evaluation of a triangular-finned absorber plate solar air heater: A Theoretical and Experimental Study. 2025;1736–1751. https://doi.org/10.5109/7388861
28. Kumar R., Saxena A. Correlation of heat transfer and flow characteristics for convex protruded triangular shaped solar air heater. Sol. Energy. 2026;307:114347. https://doi.org/10.1016/j.solener.2026.114347
29. Kumar R., Goel V. Unconventional solar air heater with triangular flow-passage: a CFD based comparative performance assessment of different cross-sectional rib-roughnesses. Renew. Energy. 2021;172:1267–1278. https://doi.org/10.1016/j.renene.2021.03.068
30. Faujdar S., Agrawal M. Computational fluid dynamics based numerical study to determine the performance of triangular solar air heater duct having perforated baffles in V-down pattern mounted underneath absorber plate. Sol. Energy. 2021;228:235–252. https://doi.org/10.1016/j.solener.2021.09.006
31. Shaik R., Punna E., Gugulothu S.K. Optimisation of thermohydraulic performance of triangular duct solar air heater with alternative dimple shaped protrusion and intrusion on the absorber plate. Therm. Sci. Eng. Prog. 2023;42:101957. https://doi.org/10.1016/j.tsep.2023.101957
32. Promvonge P., Sripattanapipat S., Jayranaiwachira N., Nakhchi M.E., Skullong S. Augmentation of solar air heater effectiveness with flapped triangular-wings. Int. J. Heat Mass Transf. 2025; 252: 127436. https://doi.org/10.1016/j.ijheatmasstransfer.2025.127436
33. Bensaci C.-E., Moummi A., de La Flor F.J.S., Jara E.A.R., Rincon-Casado A., Ruiz-Pardo A. Numerical and experimental study of the heat transfer and hydraulic performance of solar air heaters with different baffle positions. Renew. Energy. 2020; 155:1231–1244. https://doi.org/10.1016/j.renene.2020.04.017
34. Shakir A.K., Mohammed A.A., Mahmoud M.S., Abbas M.F. Numerical investigation for Y-shaped twisted inserts with trapezoidal perforations in heat exchangers. Heat Transfer. 2025;54(8):5219–5237. https://doi.org/10.1002/htj.70054
35. Mohammed A.A., Shakir A.K., Channapattana S.V. Numerical investigation of triangular Y-shaped cut twisted stripe insertion on improving the performance of heat exchangers. J. Adv. Res. Fluid Mech. Therm. Sci. 2024;124(2):220–234. https://doi.org/10.37934/arfmts.124.2.220234
36. Mohammed A.A., Mohammed A.A., Channapattana S. Numerical study of convection air currents around a hot cylinder inside a triangular cavity. Al-Nahrain J. Eng. Sci. 2023;26(2):102–115. http://doi.org/10.29194/NJES.26020102
37. Mohammed A.A., Mohammed A.A., Channapattanac S.V. Experimental investigation into natural convection heat transfer inside triangular enclosure with internal hot cylinder. Al-Nahrain J. Eng. Sci. 2023;26(3):175–185. https://doi.org/10.29194/NJES.26030175
38. Mohammed A.A., Mohammed A.A., Sadeq L.A. Heat transfer augmentation in an inclined tube using perforated conical ring inserts. J. Mech. Eng. Res. Dev. 2020; 43:1024–1752.